

This is an Open Access document downloaded from ORCA, Cardiff University's institutional repository: <https://orca.cardiff.ac.uk/id/eprint/137657/>

This is the author's version of a work that was submitted to / accepted for publication.

Citation for final published version:

Hong, John, Kim, Byung-Sung, Hou, Bo , Pak, Sangyeon, Kim, Taehun, Jang, A-Rang, Cho, Yuljae, Lee, Sanghyo, An, Geon-Hyoung, Jang, Jae Eun, Morris, Stephen M., Sohn, Jung Inn and Cha, SeungNam 2021. Room temperature wafer-scale synthesis of highly transparent, conductive CuS nanosheet films via a simple sulfur adsorption-corrosion method. *ACS Applied Materials and Interfaces* 13 (3) , pp. 4244-4252. 10.1021/acsami.0c21957

Publishers page: <http://dx.doi.org/10.1021/acsami.0c21957>

Please note:

Changes made as a result of publishing processes such as copy-editing, formatting and page numbers may not be reflected in this version. For the definitive version of this publication, please refer to the published source. You are advised to consult the publisher's version if you wish to cite this paper.

This version is being made available in accordance with publisher policies. See <http://orca.cf.ac.uk/policies.html> for usage policies. Copyright and moral rights for publications made available in ORCA are retained by the copyright holders.



1 Room Temperature Wafer-Scale Synthesis of Highly  
2 Transparent, Conductive CuS Nanosheet Films via a Simple  
3 Sulfur Adsorption-Corrosion Method

4 *John Hong<sup>a,b,†</sup>, Byung-Sung Kim<sup>a,†</sup>, Bo Hou<sup>c,†</sup>, Sangyeon Pak<sup>d</sup>, Taehun Kim<sup>d</sup>, A-Rang Jang<sup>e</sup>, Yuljae*  
5 *Cho<sup>f</sup>, Sanghyo Lee<sup>c</sup>, Geon-Hyoung An<sup>g</sup>, Jae Eun Jang<sup>h</sup>, Stephen M. Morris<sup>a</sup>, Jung Inn Sohn<sup>i</sup>,*  
6 *SeungNam Cha<sup>d,\*</sup>*

7 <sup>a</sup>Department of Engineering Science, University of Oxford, Oxford, OX1 3PJ, United Kingdom.

8 <sup>b</sup>School of Materials Science and Engineering, Kookmin University, Seoul, 02707, Republic of  
9 Korea

10 <sup>c</sup>Electrical Engineering Division, Department of Engineering, University of Cambridge, 9 JJ  
11 Thomson Avenue, Cambridge, CB3 0FA, United Kingdom.

12 <sup>d</sup>Department of Physics, Sungkyunkwan University, Suwon, 16419, Republic of Korea

13 <sup>e</sup>Department of Electrical Engineering, Semyung University, 65 Semyung-ro, Chungcheongbuk-  
14 do 27136, Republic of Korea

15 <sup>f</sup>University of Michigan – Shanghai Jiao Tong University Joint Institute, Shanghai Jiao Tong  
16 University, 800 Dong Chuan Road, Minghang District, Shanghai 200240, China

17 <sup>g</sup>Department of Energy Engineering, Gyeongnam National University of Science and Technology  
18 (GNUST), Jinju, 52725, South Korea

19 <sup>h</sup>Department of Information and Communication Engineering, Daegu Gyeongbuk Institute of  
20 Science and Technology (DGIST), Daegu, 49288, Republic of Korea.

21 <sup>i</sup>Division of Physics and Semiconductor Science, Dongguk University-Seoul, Seoul, 04620,  
22 Republic of Korea.

23

24

25 **Keywords:** transparent conductive electrodes, transition metal sulfide, vapour corrosion, scalable  
26 fabrication, flexible electronics, adsorption isotherm

1 **ABSTRACT**

2           The development of highly conductive electrodes with robust mechanical durability and  
3 clear transmittance in the visible to IR spectral range are of great importance for future  
4 wearable/flexible electronic applications. In particular, low resistivity, robust flexibility, and wide  
5 spectral transparency have a significant impact on optoelectronic performance. Herein, we  
6 introduce a new class of covellite copper monosulfide (CuS) nanosheet films as a promising  
7 candidate for soft transparent conductive electrodes (TCE). An atmospheric sulfur adsorption-  
8 corrosion phenomenon represents a key approach in our work for the achievement of wafer-scale  
9 CuS nanosheet films through systematical control of the neat Cu layer thickness ranging from 2  
10 nm to 10 nm multilayers at room temperature. These nanosheet films provide outstanding  
11 conductivity ( $\sim 25 \Omega \text{ sq}^{-1}$ ) and high transparency ( $> 80 \%$ ) in the visible to infrared region as well  
12 as distinct flexibility and long stability under air exposure, yielding a high figure-of-merit (FoM)  
13 ( $\sim 60$ ) that is comparable to that of conventional rigid metal oxide material-based TCEs. Our  
14 unique room temperature synthesis process delivers high quality CuS nanosheets on any arbitrary  
15 substrates in a short time ( $< 1 \text{ min}$ ) scale, thus guaranteeing the widespread use of highly  
16 producible and scalable device fabrication.

17

## 1 ■ INTRODUCTION

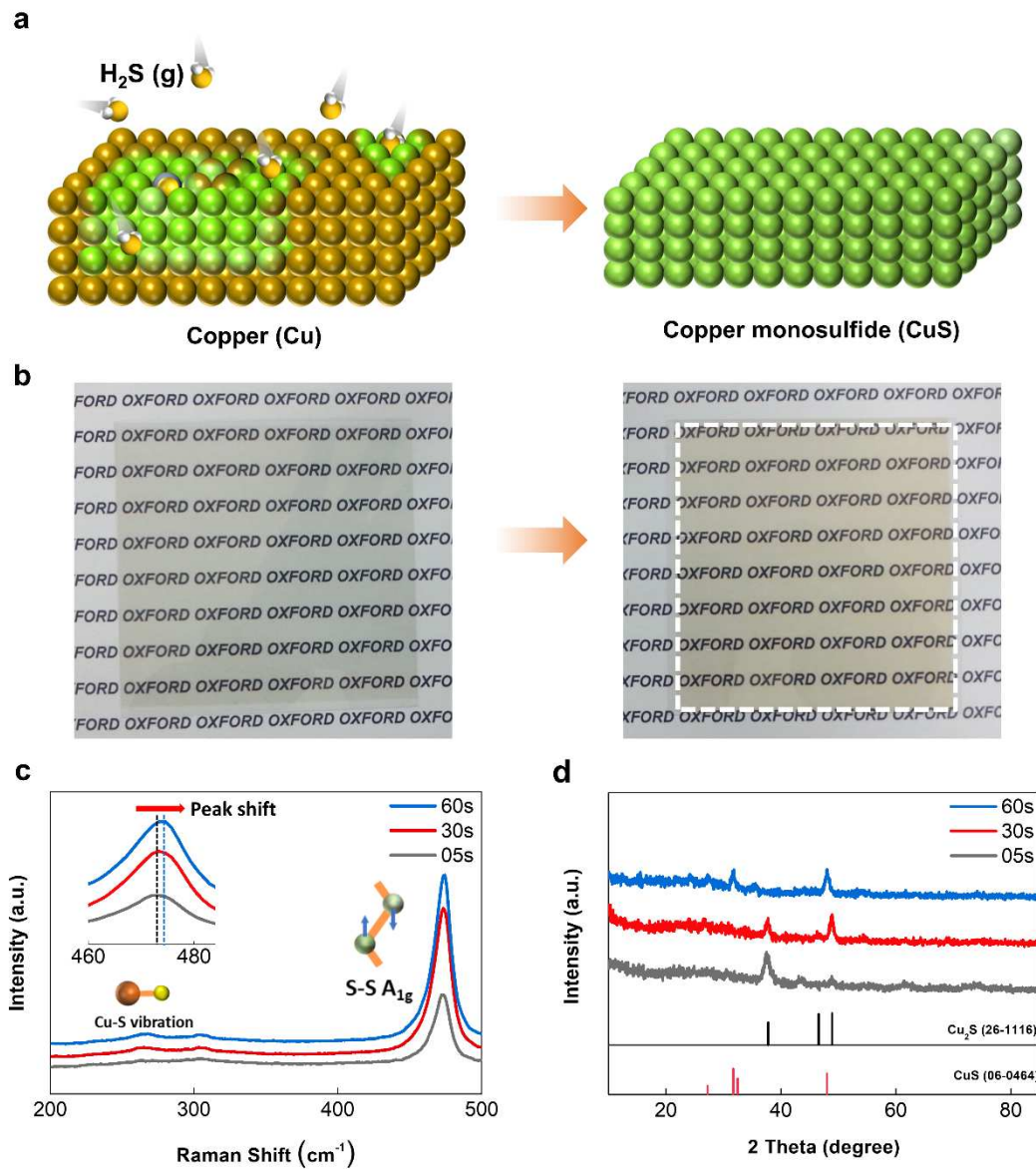
2 Following the experimental observation of highly conductive graphene, ultrathin two-  
3 dimensional (2D) materials, such as transition metal chalcogenides, black phosphorous, boron  
4 nitride, or MXenes, have also become promising alternatives for modern technological  
5 applications due to their extraordinary physical and mechanical properties at extremely low  
6 dimensions.<sup>1-7</sup> In particular, metallic 2D materials have the potential to be a new class of flexible  
7 transparent conductive electrodes (TCEs) and could be a key enabling technology in the  
8 development of next-generation flexible electronic applications such as smartphones, touch-  
9 screens, and display panels, thereby displacing the traditional transition metal oxide materials in  
10 terms of flexibility and IR transparency.<sup>8</sup> Of the numerous TCEs currently available, only graphene  
11 has been considered as a promising candidate owing to its remarkable electrical and optical  
12 properties even though there have been rapid developments in metallic 2D materials.<sup>9-11</sup> This is  
13 because there is still much to be done before these metallic 2D materials can be employed as a  
14 practical TCE. For example, the preparation of 2D materials frequently require high vacuum and  
15 high-temperature synthesis procedures (e.g. chemical vapor deposition),<sup>12-13</sup> inherently limiting the  
16 widespread use of these materials grown directly on any polymer-based flexible substrates. Thus,  
17 one of the most essential approaches was to select dry or wet transfer processes (e.g from silicon  
18 to polymer substrates after synthesis). However, these techniques have significant disadvantages  
19 in terms of unintentionally introducing surface defects and wrinkles, which negatively affect the  
20 electrical and optical features.<sup>14</sup> Therefore, finding a practical synthetic route that negates the need  
21 for additional high-temperature steps and transfer processes remains a key challenge that needs to  
22 be solved before these new metallic 2D materials can be deployed in diverse flexible and  
23 transparent electronics.

1 To date, copper sulfides ( $\text{Cu}_x\text{S}$ ) of II-VI chalcogenide materials are understood to exhibit a  
2 variety of binary phases including  $\text{Cu}_2\text{S}$  (chalcocite),  $\text{Cu}_{1.96}\text{S}$  (djurlite),  $\text{Cu}_{1.8}\text{S}$  (digenite),  $\text{Cu}_{1.75}\text{S}$   
3 (anilite), and  $\text{CuS}$  (covellite), depending on the copper stoichiometry ( $1 < x < 2$ ).<sup>15-18</sup> It is widely  
4 believed that copper vacancies in copper sulfide compounds are strongly linked with the diverse  
5 and unique optoelectronic characteristics that have been widely studied for a range of applications,  
6 such as solar cells, electromagnetic shielding layers, functional catalysts, ionic conductors, and  
7 superconductors. Among them, the copper-deficient copper monosulfide ( $\text{CuS}$ ) material shows  
8 particular promise as an impressive metallic candidate for various applications.<sup>19-22</sup> Theoretical  
9 studies indicate that the  $\text{CuS}$  possesses a graphene-like crystal structure with a  $P63/mmc$  space  
10 group and highly metallic conductivity perpendicular to the  $c$ -axis direction. Despite the large body  
11 of work on  $\text{CuS}$  nanosheets, there are still limitations with regards to the use of low temperature  
12 fabrication procedures, the scalability of  $\text{CuS}$  nanosheet films, controlling the thickness and  
13 achieving high conductivity values close to the theoretical limit. In fact, overcoming these  
14 limitations is essential for their practical realization as a TCE candidate. In addition, finding a new  
15 synthetic procedure that results in the tailoring of the  $\text{CuS}$  composition is challenging due to its  
16 stoichiometry-dependent properties.

17 Herein, we introduce a wafer-scale synthesis method of highly crystalline  $\text{CuS}$  nanosheet  
18 films which has the potential to be an alternative TCE by employing an atmospheric sulfur  
19 adsorption-corrosion reaction approach at room temperature (RT). Specifically, the high anion  
20 reactive ability of copper transition metals with oxygen or sulfur atoms even at RT ensures the  
21 synthesis of high quality, uniform, and ultra-thin  $\text{CuS}$  nanosheet films (NF) in the range of 2 to 10  
22 nm. The  $\text{CuS}$  nanosheets exhibit not only a low sheet resistance of  $\sim 25 \Omega \text{ sq}^{-1}$  but also excellent  
23 optical transparency in the visible to infrared (IR) region of  $\sim 80\%$ , which is much more transparent

1 than conventional oxide films in this region of the spectrum.<sup>23</sup> The calculated figure-of-merit  
2 (FoM) is found to reach values of  $\sim 60$ , which is beyond the minimum industrial requirement for  
3 practical applications. Remarkably, these TCE parameters can be preserved even when subjected  
4 to large strains, which is particularly important for future flexible electronics. Thus, this simple  
5 room temperature chemical deposition process could be generalized and extended towards highly  
6 uniform and large scale CuS NFs on any arbitrary substrate for advanced flexible optoelectronic  
7 devices, including a promising TCE candidate that could be deployed in various electronic  
8 applications (IR device and quantum dot light emitting diodes).

1 ■ RESULTS AND DISCUSSIONS



2

3 **Figure 1.** (a) Schematic illustration of the sulfurization process in the CuS nanosheets. (b) Optical  
 4 images of a 2 nm-Cu nanosheet film and the corresponding CuS nanosheet films before and after  
 5 the sulfurization process. (c) Raman spectra of the CuS samples after sulfurization process for  
 6 different time durations (5 sec, 30 sec and 60 sec). (d) XRD results from CuS samples for different  
 7 duration times (5 sec, 30 sec and 60 sec).

1 A schematic illustration of the fabrication procedure is shown in **Figure 1a**. A facile, one-  
2 step sulfurization method was used to fabricate conductive and transparent CuS nanosheets. Before  
3 the sulfurization process, the Cu metal thin nanosheets were carefully deposited on target  
4 substrates (glass or PET (polyethylene terephthalate)) by a simple evaporation technique. The  
5 thickness of Cu (ranging from ~ 2 to 10 nm) was precisely controlled by the evaporation time.  
6 Subsequently, the Cu metal films were directly exposed to H<sub>2</sub>S gas that was evaporated from the  
7 ammonium sulfide solution. The continuous sulfur supply from the solution readily transforms the  
8 pure Cu films into transparent CuS nanosheet films at room temperature (**Figure 1b**). As reported  
9 in the literature, chalcocite Cu<sub>2</sub>S and covellite CuS are both harvestable phases at room  
10 temperature, but the formation of Cu<sub>2</sub>S in bulk form has mainly been reported only in sulfur-  
11 limiting environments.<sup>24</sup> In contrast to the bulk, the adequate supply of sulfur onto limited Cu  
12 dimensions (nm thickness) plays a critical role in forming the covellite CuS phase instead of Cu<sub>2</sub>S.  
13 The overall atmospheric sulfurization in the presence of H<sub>2</sub>S gas take places according to the  
14 following reaction:<sup>25</sup>

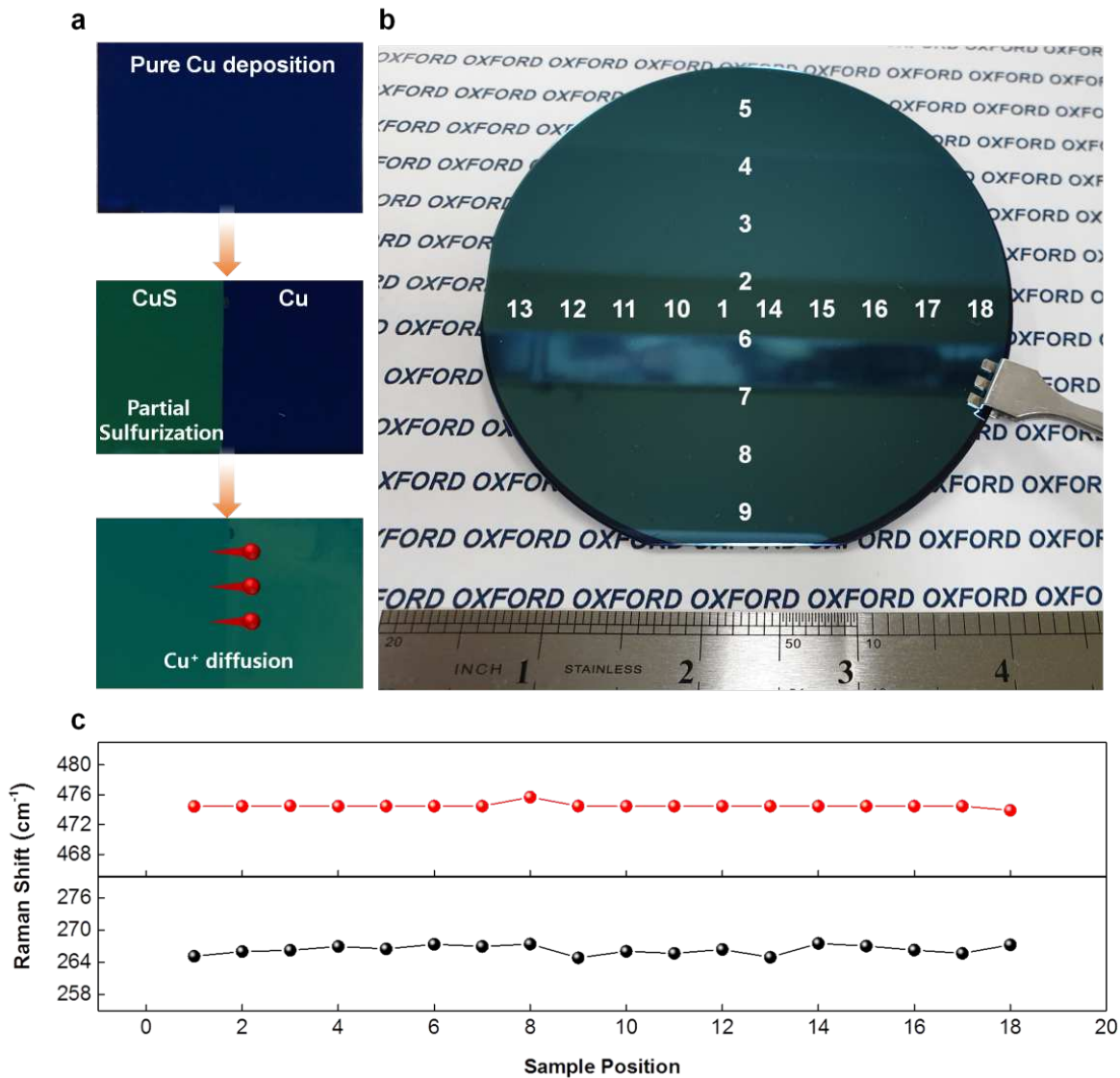


16 Usually, highly reactive H<sub>2</sub>S can be adsorbed onto a Cu surface, resulting in Cu<sub>2</sub>S as the  
17 main corrosion product. Moreover, the reaction of sulfur ions at the gas/sulfide interface results in  
18 the depletion of cuprous vacancies, which transport through the sulfide layer during the growth of  
19 the Cu<sub>2</sub>S phase.<sup>26,27</sup> However, it was found that further reaction with the continuous sulfur supply  
20 from a gas atmosphere leads to the top layer being converted to the covellite CuS phase. This can  
21 be further confirmed by the sulfurization of a Cu foil with the sulfurization process (**Figure S1**).  
22 As shown in **Figure S1a**, different exposure times to the sulfur gas induces different surface  
23 conditions on the Cu foil with different color changes. Within 5 to 30 sec sulfurization time, most



1 of the surface of the Cu foil is conjugated with the Cu<sub>2</sub>S phase. After 60 sec, the surface turned  
2 into the blueish CuS phase. To check the surface states along with a small depth of the Cu foil, the  
3 thin nanosheets from the reacted Cu foil were cleaved and transferred to a SiO<sub>2</sub> wafer (**Figure S1b**)  
4 via a wet-transfer process. **Figure S1c** shows the optical image of the transferred CuS nanosheets  
5 from the Cu foil. Raman analysis was carried out to check the transferred CuS nanosheets, and the  
6 peak of the in-plane Cu-S vibration at 266 cm<sup>-1</sup> for CuS crystal, ensuring the successful conversion  
7 of Cu or Cu<sub>2</sub>S under the sufficient supply of sulfur gas.<sup>28,29</sup> In addition, measurements from time-  
8 of-flight secondary-ion mass spectrometry (TOF-SIMS) suggests the fast out-diffusion of the  
9 cuprous vacancy and sulfur atom on the Cu foil for short timescales (< 1 min) even at room  
10 temperature (**Figure S2a**).

11 To investigate the phase-transition mechanism in the CuS samples, Raman and XRD (X-  
12 Ray Diffraction) measurements were systematically carried out with 10 nm-Cu nanosheets for  
13 different sulfurization times. A dominant peak at 472 cm<sup>-1</sup> for the Cu film exposed for 5 sec was  
14 identified to be the Cu<sub>2</sub>S phase, which gradually shifted to 474 cm<sup>-1</sup> corresponding to the out-of-  
15 plane S-S vibration (A<sub>1g</sub> mode) in the covellite CuS phase (**Figure 1c** and inset).<sup>30</sup> The peak of the  
16 in-plane Cu-S vibration at 266 cm<sup>-1</sup> is also intensified according to an increased sulfurization time  
17 (**Figure S2b** and **2c**). The peak shifts at 474 cm<sup>-1</sup> as well as the enhanced peak intensity at 266 cm<sup>-1</sup>  
18 indicate that with the appropriate supply of sulfur to the limited Cu dimensions is a key parameter  
19 in generating covellite CuS from Cu sources. To further support our proposed mechanism, XRD  
20 measurements for the corresponding sulfurization times and a similar variation tendency (**Figure**  
21 **1d** and **Figure S2d**) was conducted. The results also demonstrate the successful transition from  
22 cubic Cu (JCPDS Card No. 85-1326) and chalcocite Cu<sub>2</sub>S (JCPDS Card No. 26-1116) to covellite  
23 CuS (JCPDS Card No. 06-0464) at room temperature after longer sulfurization times.<sup>31,32</sup>



1

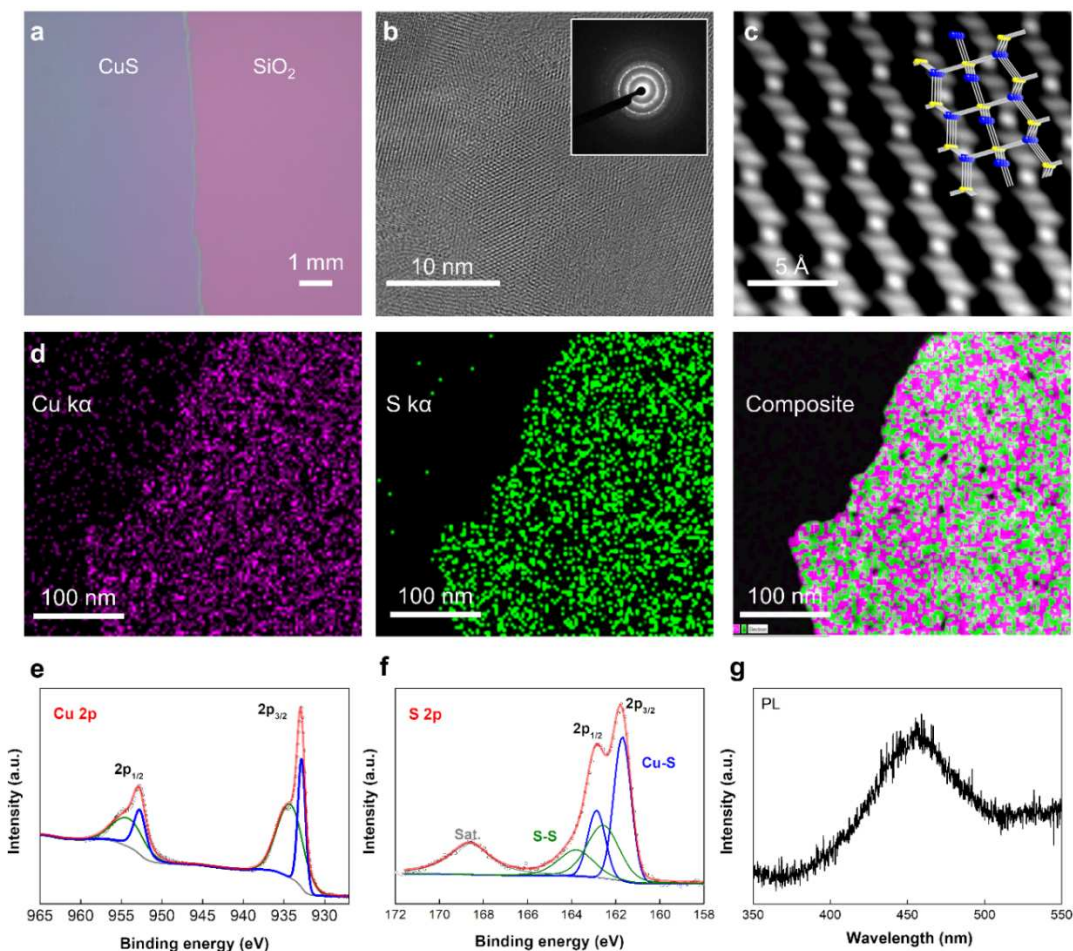
2 **Figure 2.** (a) Lateral sulfur diffusion in Cu/CuS nanosheet films. (b) Large scale fabrication of a  
 3 CuS nanosheet on a SiO<sub>2</sub>/Si substrate. (c) Raman shifts at selected points across the sample as  
 4 labelled in **Figure 2b**.

5

6 As shown in **Figure 2a**, 10 nm-Cu films were deposited onto a SiO<sub>2</sub> substrate and the partial  
 7 area of the deposited Cu films was initiated via a sulfurization process. The straight line in the

1 optical image represents the boundary between the Cu and CuS films. After a few hours, an area  
2 of the Cu film on the boundary line was also converted into CuS. This is due to the high sulfur and  
3 cuprous Cu diffusivity from the localized sulfur atoms. Based on the scalable and facile vapor-  
4 based sulfurization method and diffusion of cuprous Cu and S, large wafer-scale CuS nanosheet  
5 films can also be successfully synthesized on a 4-inch scale Si wafer (**Figure 2b**). The as-grown  
6 CuS nanosheets were continuously and uniformly fabricated over a large area of the Si wafer.  
7 **Figure 2c** exhibits the representative Raman spectrum analyses on the randomly selected 18  
8 different points on the CuS samples in order to quantitatively confirm the uniformity over a large  
9 area. As seen, the peak positions of the S-S (A1g mode) and Cu-S modes remain identical in all  
10 the spectra, which are centered at  $\sim 474\text{ cm}^{-1}$  and  $\sim 266\text{ cm}^{-1}$ , respectively, confirming the excellent  
11 uniformity of CuS on the substrate. **Figure S3** shows the areal AFM scanning image, which  
12 indicates a uniform surface of 10 nm-CuS on the  $\text{SiO}_2$  substrate.

13

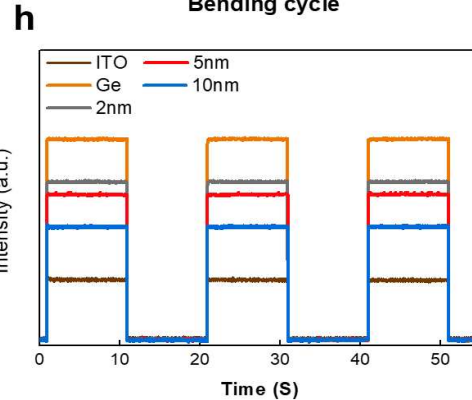
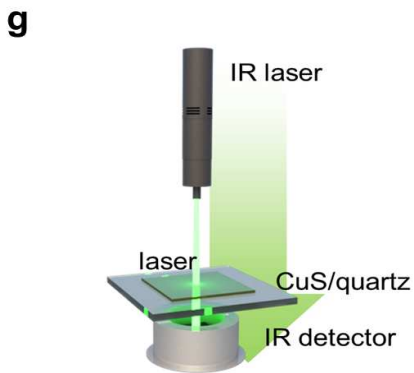
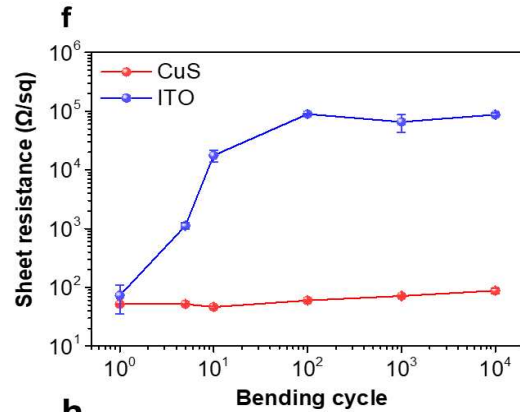
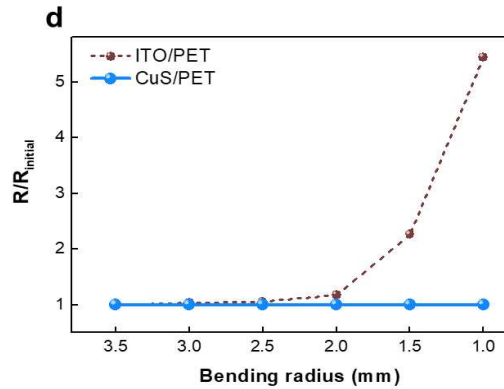
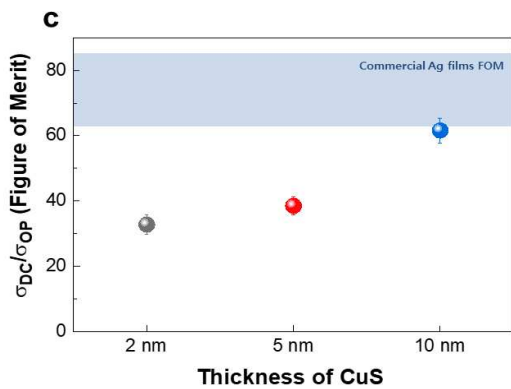
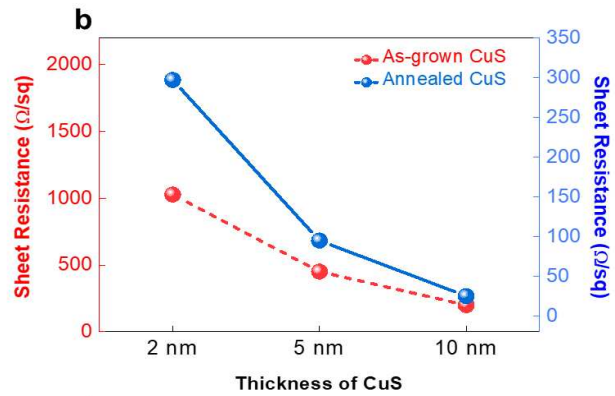
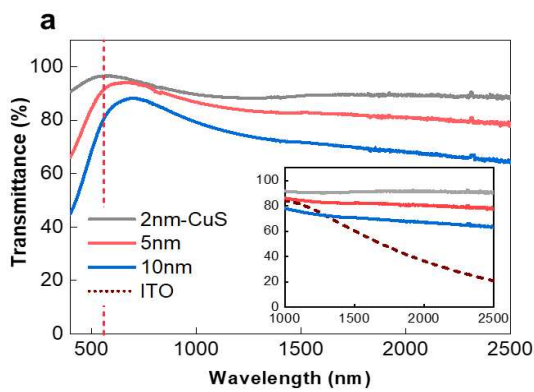


1  
 2 **Figure 3.** (a) Optical microscopy image of a CuS nanosheet on a SiO<sub>2</sub>/Si substrate. (b) TEM image  
 3 of CuS. Inset image shows an SAED image of CuS (c) ARM HAADF-STEM image of CuS. (d)  
 4 Mapping images of Cu  $\kappa\alpha$ , S  $\kappa\alpha$  and composite of CuS. XPS spectra of (e) Cu 2p and (f) S 2p of  
 5 CuS. (g) PL spectra of CuS.

6  
 7 The crystal nature of CuS was analyzed directly using atomic-resolution high-angle annular  
 8 dark-field scanning transmission electron microscopy (ARM HAADF-STEM). **Figure 3a** shows  
 9 the wet transferred CuS nanosheet films on a SiO<sub>2</sub> substrate. The nanosheets were further  
 10 transferred onto a gold grid for TEM analysis. A well-organized honeycomb structure (**Figure 3b**),

1 along with corresponding spotty selected-area ring patterns (inset of **Figure 3b**) suggests that the  
2 atomically thin covellite crystal of the as-prepared CuS is indeed an atomically thin covellite  
3 crystal. Characteristic atomic-scale lattice images were taken through (100)-axis, which shows the  
4 consistent spatial distribution of the Cu and S atoms (**Figure 3c**) with the atomic covellite model  
5 (inset of **Figure 3c**). The stoichiometric phase distribution of CuS is determined through HAADF-  
6 STEM energy-dispersive X-ray spectroscopy mapping (**Figure 3d**), which exhibit a homogeneous  
7 distribution of the Cu and S elements over CuS. X-ray photoelectron spectroscopy (XPS) analysis  
8 was also carried out to further verify the chemical states of CuS (**Figure S4**). **Figures 3e** and **3f**  
9 show the high-resolution XPS spectra of the S 2p and Cu 2p peak regions, respectively. The  
10 locations of the binding energy peaks of Cu 2p at 932.8 and 934.5 eV are indicative of the chemical  
11 states of CuS.<sup>33</sup>

12         The S 2p fitting peaks can be deconvoluted into two main deconvoluted doublets. The two  
13 main peak doublets are centered at 161.6 eV and 162.6 eV, which are typical values for metal  
14 sulfides and can be assigned to sulfide and disulfide, respectively, implying that the ionic model  
15 of the as-prepared nanosheets is  $(\text{Cu}_2)^{2+}(\text{Cu})^{2+}(\text{S}_2)^{2-}(\text{S})^2$ .<sup>34</sup> These findings also indicate that our  
16 samples have been successfully converted from cubic copper to covellite CuS with high crystalline  
17 quality. The optical properties of the CuS nanosheets were characterized by photoluminescence  
18 (PL, wavelength 266 nm, 20 mW) spectroscopy. **Figure 3g** represents the emission spectra of the  
19 10nm-CuS sample. The emission peak is centered at  $\sim 450$  nm, which is close to the reported PL  
20 emission peaks of bulk CuS and ultrathin CuS, demonstrating that, after the sulfurization process,  
21 the pure Cu is converted to the CuS composition.<sup>35</sup> The thickness of the CuS nanosheets were also  
22 characterized using an AFM as shown in **Figure S5**.



1 **Figure 4.** (a) Transmission spectrum of CuS and ITO films. Inset shows the transmittance curve  
2 of CuS and ITO films for just the IR region (b) Sheet resistance values of CuS nanosheet films  
3 before and after thermal treatment at 150 °C (c) FoM values for the 2 nm-, 5 nm- and 10 nm-CuS  
4 nanosheet films. (d) Sheet resistance of CuS and ITO electrodes for different bending radii. Inset  
5 images show that the CuS electrode can still function even when it is bended. (e) An optical image  
6 of a bending test machine. (f) Sheet resistance of CuS and ITO films after the 10,000 bending  
7 cycles. (g) Schematic illustration of the infrared laser penetration test. (h) On-off IR photoswitch  
8 curve for the CuS and ITO electrodes.

9  
10 The electrical, optical and mechanical properties of the CuS film as a flexible and  
11 transparent conductive electrode were determined as shown in **Figure 4**. The optical transmittance  
12 of CuS on a glass substrate was measured using a spectrometer covering the visible to infrared  
13 region (450 nm to 2500 nm) (**Figure 4a**). The transmittance of CuS at 550 nm is clearly comparable  
14 to that of the ITO films, which are ~96.1%, ~90.7% and ~79.4% for the 2 nm-CuS, 5 nm-CuS and  
15 10 nm-CuS films, respectively. Moreover, the CuS nanosheet films have superior transmittance in  
16 the infrared region from 1000 to 2500 nm (~ 80%). As shown in the inset of **Figure 4a**, the  
17 commercial ITO films have poor transmittance in this region (~ 40%) especially at 2000 nm. Based  
18 upon this optical property, CuS nanosheets are clearly an appealing candidate for optoelectronic  
19 devices in the visible to infrared region. Moreover, the transmittance of CuS in the visible region  
20 below 600nm drop sharply.<sup>36-39</sup>

21 **Figure 4b** shows the sheet resistance values for 2 nm-, 5 nm-, and 10 nm-CuS nanosheets  
22 using the four-point resistance measurement. The electrical conductivity of CuS dramatically

1 improved with increasing thickness, while the transparency decreased slightly from 2 nm- to 10  
2 nm-CuS. The average sheet resistance values of CuS are found to be 297.2  $\Omega$  sq<sup>-1</sup>, 94.9  $\Omega$  sq<sup>-1</sup> and  
3 25.1  $\Omega$  sq<sup>-1</sup>, respectively, following thermal treatment at 150 °C for 5 min under inert gas (**Figure**  
4 **S6**). These high conductivity values correlate with the metallic-like properties of as-grown CuS.  
5 The further crystallization and atomic ordering of the as-prepared CuS can be induced by simple  
6 heat treatment at 150 °C. The calculated average figure of merits (FoMs) of the 2 nm-, 5 nm-, and  
7 10 nm-CuS nanosheets at 550 nm are found to be 31.9, 39.8 and 61.6, respectively, which are  
8 higher than the industrial commercialization standard for optical applications (**Figure 4c**).<sup>40</sup> The  
9 FoMs in the IR region are much higher than that of commercial TCEs (usually less than 20).  
10 Commercial nano silver wire transparent conductive films (NSWTCFs) with a transparency of  
11 ~92% and a sheet resistance 50~70  $\Omega$  sq<sup>-1</sup>were purchased and the electrical and mechanical  
12 properties of NSWTCF were tested to compare the performance of CuS (**Figure S7**). To investigate  
13 the electric stability of CuS under air exposure, the sheet resistances of the CuS and pure Cu films  
14 were examined. As shown in **Figure S8a**, on the basis of XRD results, the Cu<sub>x</sub>O peaks were  
15 identified on the Cu films after few days under air. These partially oxidized films are not well  
16 crystallized. Moreover, in terms of electrical conductivity, as shown in **Figure S8b**, the CuS films  
17 can well maintain its original conductivity, but the conductivity of the as-deposited Cu films was  
18 dramatically decreased after 7 days

19 Mechanical and durability assessment of the CuS nanosheets was carried out by measuring  
20 the variation in the sheet resistance. The relative resistance values of the CuS and ITO films before  
21 and after bending were evaluated (**Figure 4d**). While the relative resistance of the ITO films  
22 drastically increased according to a decrease in the bending radius from 3.5 mm to 1.0 mm. The  
23 relative resistance of the CuS nanosheets remains nearly unchanged. Moreover, for the durability



1 test, the slope of the two terminal I-V curves was well-maintained even though the CuS nanosheet  
2 films were bended, twisted, and even crumpled (**Figures S9a and 9b**). The experimental results  
3 show that the CuS nanosheets possess good optical and electrical properties as well as superior  
4 bending properties with high degree of durability.

5 To investigate the mechanical stability of CuS, as shown in Figure 4e, the CuS and ITO  
6 films were folded 10,000 times using a home-made automatic fold testing machine, and the sheet  
7 resistances of both films were measured. As shown in Figure 4f, the resistance of the ITO films  
8 has been dropped dramatically after the 10,000 cycles. Instead, the CuS films can maintain its  
9 original sheet resistance even after the 10,000 folds, which demonstrating its superior mechanical  
10 stability of CuS against the applied stress. **Figure 4g** shows a schematic illustration of an IR light  
11 transmitting test using a 1550 nm incident laser on the film and a germanium (Ge)-IR detector.  
12 The initial intensity of the laser was compared with that of the incident laser after penetrating the  
13 CuS nanosheet films, ITO or glass substrates and the IR laser was turned on and off within a 10  
14 sec time frame. Compared to the ITO films and glass, the readout intensity of the IR laser exhibited  
15 negligible attenuation after transmitting through the CuS nanosheets. A monotonic IR  
16 transmittance phenomena was observed in our thickness-dependent studies. As shown in **Figure**  
17 **4h**, the thinnest CuS nanosheet film shows the highest IR transmittance beyond the others which  
18 indicates that the atomic-thick CuS nanosheet has negligible IR absorption or reflection. These  
19 results imply that the CuS electrodes can be potentially applied to IR optical and electronic  
20 applications as a promising electrode candidate.

21 To further examine the eligibility of the CuS nanosheets as one of the possible TCE in  
22 optical electronic applications, we fabricated cadmium selenide (CdSe)/zinc sulfide (ZnS)  
23 core/shell quantum dot light emitting diodes (QD-LEDs) using a CuS electrode as the anode (the

1 charge transfer layer). **Figure S9c** shows a schematic illustration of the QD-LEDs. On the CuS  
2 electrode, a 50 nm poly(ethylenedioxythiophene):polystyrene sulphonate(PEDOT:PSS) was used  
3 as the hole injection layer (HIL), a 50 nm poly[(9,9-dioctylfluorenyl-2,7-diyl)-co-(4,4-(N-(4-sec-  
4 butylphenyl)) diphenylamine)] (TFB) layer was used as the hole transfer layer (HTL). The red-  
5 colored CdSe/ZnS QD films (30 nm) were spin-coated onto the as-prepared substrate. Finally, a  
6 100 nm zinc oxide (ZnO) was used as the electron transfer layer (ETL) and an Al cathode were  
7 deposited on the QD films. Currently, the optimization of experimental parameters such as the  
8 coating of the QDs and the deposition of various transfer layers on the CuS electrodes is still under  
9 investigation for enhanced electroluminescent performance such as the external quantum  
10 efficiency. Nevertheless, the experimental characterization and the device results strongly  
11 recommend the use of CuS nanosheets and the simple sulfurization process at room temperature  
12 would establish a useful route for future optoelectronic devices when flexibility is a key  
13 requirement. Figure S9d shows the additional lighting image for 10 nm CuS/QDLED under the  
14 characterization. Figure S9e-f shows the I-V and EQE curve of the device. The estimated  
15 maximum luminescence is 1240.0 cd m<sup>-2</sup>. The electrical properties of the CuS samples were  
16 measured by Hall Effect technique with tungsten (W) electrode contacts in a square sample of the  
17 1x1 cm<sup>2</sup> with Van der Pauw configuration. All the samples exhibited p-type behavior (Average  
18 carrier concentration:  $2.47 \times 10^{22}$  cm<sup>-3</sup> & Average mobility: 1.28 cm<sup>2</sup> V<sup>-1</sup>s<sup>-1</sup>) and showed the semi-  
19 metal behavior (Table S1).

20

1 ■ **CONCLUSION**

2           In conclusion, wafer-scale metallic CuS nanosheets with high transparency, conductivity  
3 and excellent flexibility have been synthesized directly onto various substrates via an atmospheric  
4 sulfur adsorption-corrosion reaction. The gas sulfurization process has been utilized to grow high-  
5 quality CuS sheets with atomic-thickness controllability (from monolayers of 2 nm to multilayers  
6 of 10 nm). We have demonstrated that the CuS electrodes show high optical transparency and  
7 conductivity with FoM values close to 60, which readily surpass the industrial commercialization  
8 requirements for optical applications. Moreover, the CuS electrodes can be successfully applied to  
9 various optical applications such as apertures for IR detectors and TCEs for QD-LEDs. Our  
10 findings are of significant importance in the development of new TCEs for flexible optoelectronic  
11 applications with scalable productivity.

12

## 1 ■ MATERIALS AND METHODS

2 **Synthesis of CuS Nanosheets.** Before sulfurization process, pure copper (Cu) films with different  
3 thicknesses were deposited on a Si/SiO<sub>2</sub> substrate, a glass or a flexible polyethylene terephthalate  
4 (PET) polymer substrate by thermal evaporation in high vacuum. The thicknesses of the Cu films  
5 were carefully tailored by a deposition meter in the machine. The deposited Cu films were directly  
6 exposed to the vaporized sulfur gas from an ammonium sulfide solution (20 wt.%) which was  
7 purchased from Sigma-Aldrich followed by 1~3 min of static displacement above the solution  
8 according to the thicknesses of CuS without any heat treatment in a lab environment at 25 °C. For  
9 the further conductive enhancement and crystallization, the CuS nanosheet films on the substrate  
10 were placed in the CVD furnace under Ar and annealed at 150 °C for 1~5 min according to the  
11 desired thickness of CuS with rapid cooling processes.

12 **Material and Electrical Characterization.** The optical and crystal properties of CuS nanosheets  
13 were characterized using scanning electron microscopy (SEM, Hitachi S-4300), transmission  
14 electron microscopy (TEM, JEOL JEM-2200MCO FEGTEM), ultraviolet–visible spectroscopy  
15 (UV-Vis, Varian Cary 5000), Raman spectroscopy (Horiba LabRAM ARAMIS Imaging Confocal  
16 Raman Microscope), time of flight secondary ion mass spectrometry (TOF-SIMS-5, Germany),  
17 atomic force microscope (AFM, Veeco Dimension 3100) photoluminescence spectroscopy (PL,  
18 Fluorolog, Horiba Jobin Yvon) and high-resolution X-ray diffraction (XRD, Rigaku Medel  
19 Smartlab). To check the oxidation states of CuS, X-ray photon electron spectroscopy (XPS) was  
20 conducted using a Thermo Scientific K-Alpha XPS instrument with a micro-focused  
21 monochromatic Al X-ray source. The spectrometer was adjusted to align to a binding energy of  
22 284.5 eV for the C 1s. The (opto)electronic properties of the CuS nanosheets and corresponding  
23 devices were measured using the electrical characterization system (4200-SCS, Keithley), LeCroy

1 HD4000 high-definition oscilloscope, and 6-probe Cascade Microtech probe station.

2

### 3 ■ **ACKNOWLEDGEMENT**

4 This work was supported by the National Research Foundation (NRF) of Korea  
5 (2019R1A2C1005930), and the European Research Council under the European Union's Seventh  
6 Framework Programme (FP/2007-2013)/Grant Agreement no. 685758.

7

### 8 ■ **ASSOCIATED CONTENT**

#### 9 **Supporting Information**

10 Photographs and optical images of CuS, Raman spectra, SIMS spectra, XRD, AFM, XPS, AFM  
11 Height profiles, Sheet resistance values for 2 nm-, 5 nm- and 10 nm-CuS, Sheet resistances of  
12 commercial NSWTCF, Time-dependent sheet resistance of Cu and CuS, Schematic illustration of  
13 QD-LED with CuS, and I-V and EQE curve for CuS-10 nm/QD-LED

14

### 15 ■ **AUTHOR INFORMATION**

#### 16 **Corresponding author**

17 SeungNam Cha, \*E-mail address: [chasn@skku.edu](mailto:chasn@skku.edu), Tel: +82-31-299-4546

#### 18 **ORCID**

19 John Hong: 0000-0002-1513-8622

20 Bo Hou: 0000-0001-9918-8223

21 Sangyeon Pak: 0000-0003-1765-3043

22 Taehun Kim: 0000-0002-3695-4071

23 A-Rang Jang: 0000-0002-0758-9757

24 Yuljae Cho: 0000-0003-2976-0604

- 1 Sanghyo Lee: 0000-0002-4723-9612
- 2 Geon-Hyoung An: 0000-0003-0211-7993
- 3 Jae Eun Jang: 0000-0002-8523-1785
- 4 Stephen M. Morris: 0000-0001-8294-9225
- 5 Jung Inn Sohn: 0000-0002-3155-4327
- 6 SeungNam Cha: 0000-0001-6284-8312

7

8 **Author Contributions**

9 † John Hong, Byung-Sung Kim, Bo Hou contributed equally to the work

10  
11  
12  
13  
14  
15  
16

1 ■ REFERENCES

- 2 [1] Allen, M.; Tung, V.; Kaner, R. Honeycomb Carbon: A Review of Graphene. *Chem. Rev.* **2010**,  
3 *110*, 132-145.
- 4 [2] Das, S.; Robinson, J.; Dubey, M.; Terrones, H.; Terrones, M. Beyond Graphene: Progress in  
5 Novel Two-Dimensional Materials and van der Waals Solids. *Annu. Rev. Mater. Res.* **2015**, *45*, 1-  
6 27.
- 7 [3] Zhang, K.; Feng, Y.; Wang, F.; Yang, Z.; Wang, J. Two-Dimensional Hexagonal Boron Nitride  
8 (2D-hBN): Synthesis, Properties and Applications. *J. Mater. Chem. C* **2017**, *5*, 11992-12022.
- 9 [4] Liu, H.; Hu, K.; Yan, D.; Chen, R.; Zou, Y.; Liu, H.; Wang, S. Recent Advances on Black  
10 Phosphorus for Energy Storage, Catalysis, and Sensor Applications. *Adv. Mater.*  
11 **2018**, *30*, 1800295 (1-22).
- 12 [5] Wang, Q. H.; Kalantar-Zadeh, K.; Kis, A.; Coleman, J.; Strano, M. Electronics and  
13 Optoelectronics of Two-Dimensional Transition Metal Dichalcogenides. *Nat. Nanotechnol.*  
14 **2012**, *7*, 699-712.
- 15 [6] Shi, S.; Sun, Z.; Hu, Y. H. Synthesis, Stabilization and Applications of 2-Dimensional 1T  
16 Metallic MoS<sub>2</sub>. *J. Mater. Chem. A* **2018**, *6*, 23932-23977.
- 17 [7] Anasori, B.; Lukatskaya, M.; Gogotsi, Y. 2D Metal Carbides and Nitrides (MXenes) for Energy  
18 Storage. *Nat. Rev. Mater.* **2017**, *2*, 16098 (1-17).
- 19 [8] Yoon, J.; Park, W.; Bae, G.-Y.; Kim, Y.; Jang, H. S.; Hyun, Y.; Lim, S. K.; Kahng, Y. H.;  
20 Hong, W.-K.; Lee, B. H.; Ko, H. C. Highly Flexible and Transparent Multilayer MoS<sub>2</sub> Transistors  
21 with Graphene Electrodes. *Small* **2013**, *9*, 3295 (1-6).

- 1 [9] Kuzum, D.; Takano, H.; Shim, E.; Reed, J.; Juul, H.; Richardson, A.; Vries, J.; Bink, H.;  
2 Dichter, M.; Lucas, T.; Coulter, D.; Cubukcu, E.; Litt, B. Transparent and Flexible Low Noise  
3 Graphene Electrodes for Simultaneous Electrophysiology and Neuroimaging. *Nat.*  
4 *Commun.* **2014**, *5*, 5259 (1-10).
- 5 [10] Rana, K.; Singh, J.; Ahn, J.-H. A Graphene-Based Transparent Electrode for Use in Flexible  
6 Optoelectronic Devices. *J. Mater. Chem. C* **2014**, *2*, 2646-2656.
- 7 [11] Tan, R. K. L.; Reeves, S.; Hashemi, N.; Thomas, D. G.; Kavak, E.; Montazami, R.; Hashemi,  
8 N. Graphene as a Flexible Electrode: Review of Fabrication Approaches. *J. Mater. Chem. A* **2017**,  
9 *5*, 17777-17803.
- 10 [12] Liu, L.; Wu, J.; Wu, L.; Ye, M.; Liu, X.; Wang, Q.; Hou, S.; Lu, P.; Sun, L.; Zheng, J.; Xing,  
11 L.; Gu, L.; Jiang, X.; Xie, L.; Jiao, L. Phase-selective Synthesis of 1T' MoS<sub>2</sub> Monolayers and  
12 Heterophase Bilayers. *Nat. Mater.* **2018**, *17*, 1108-1114.
- 13 [13] Rao, C. N. R.; Matte, H. S. S.; Subrahmanyam, K. S. Synthesis and Selected Properties of  
14 Graphene and Graphene Mimics. *Acc. Chem. Res.* **2013**, *46*, 149-159.
- 15 [14] Suk, J. W.; Kitt, A.; Magnuson, C.; Hao, Y.; Ahmed, S.; An, J.; Swan, A.; Goldberg, B.;  
16 Ruoff, R. Transfer of CVD-Grown Monolayer Graphene onto Arbitrary Substrates *ACS*  
17 *Nano* **2011**, *5*, 6916-6924.
- 18 [15] Hong, J.; Kim, B.-S.; Yang, S.; Jang, A.-R.; Lee, Y.-W.; Pak, S.; Lee, S.; Cho, Y.; Kang, D.;  
19 Shin, H. S.; Hong, J. P.; Morris, S.; Cha, S.; Sohn, J. I.; Kim, J. M. Chalcogenide Solution-  
20 Mediated Activation Protocol for Scalable and Ultrafast Synthesis of Single-Crystalline 1-D  
21 Copper Sulfide for Supercapacitors. *J. Mater. Chem. A* **2019**, *7*, 2529-2535.



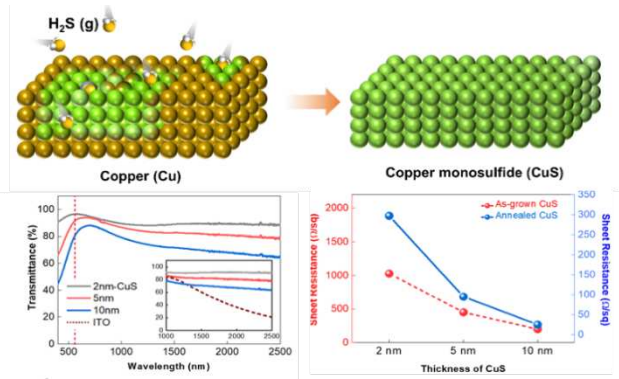
- 1 [16] Roy, P.; Srivastava, S. K. Nanostructured Copper Sulfides: Synthesis, Properties and  
2 Applications. *Crystengcomm.* **2015**, *17*, 7801-7815.
- 3 [17] Sun, S.; Li, P.; Liang, S.; Yang, Z. Diversified Copper Sulfide (Cu<sub>2-x</sub>S) Micro-  
4 /Nanostructures: A Comprehensive Review on Synthesis, Modifications and Applications  
5 *Nanoscale* **2017**, *9*, 11357-11404.
- 6 [18] Mousavi-Kamazani, M.; Zarghami, Z.; Salavati-Niasari, M. Facile and Novel Chemical  
7 Synthesis, Characterization, and Formation Mechanism of Copper Sulfide (Cu<sub>2</sub>S, Cu<sub>2</sub>S/CuS, CuS)  
8 Nanostructures for Increasing the Efficiency of Solar Cells. *J. Phys. Chem. C* **2016**, *120*, 2096-  
9 2108.
- 10 [19] Nozaki, H.; Shibata, K.; Ohhashi, N. Metallic Hole Conduction in CuS. *J. Solid. State.*  
11 *Chem.* **1991**, *91*, 306-311.
- 12 [20] Soares, A.; Santos, E.; Morales-Garcia, A.; Heine, T.; Abreu, H.; Duarte, H. Two-  
13 Dimensional Crystal CuS—Electronic and Structural Properties. *2D Mater.* **2017**, *4*, 015041 (1-  
14 7).
- 15 [21] Lee, Y.-W.; Kim, B.-S.; Hong, J.; Lee, J.; Pak, S.; Jang, H.-S.; Whang, D.; Cha, S.; Sohn, J.  
16 I.; Kim, J. M. A Pseudo-Capacitive Chalcogenide-based Electrode with Dense 1-Dimensional  
17 Nanoarrays for Enhanced Energy Density in Asymmetric Supercapacitors. *J. Mater. Chem.*  
18 *A* **2016**, *4*, 10084-10090.
- 19 [22] Sakamoto, T.; Sunamura, H.; Kawaura, H.; Hasegawa, T.; Nakayama, T.; Aono, M.  
20 Nanometer-Scale Switches Using Copper Sulfide *Appl. Phys. Lett.* **2003**, *82*, 3032-3034.

- 1 [23] Bitla, Y.; Chen, C.; Lee, H.-C.; Do, T. H.; Ma, C.-H.; Qui, L. V.; Huang, C.-W.; Wu, W.-W.;  
2 Chang, L.; Chiu, P.-W.; Chu, Y.-H. Oxide Heteroepitaxy for Flexible Optoelectronics. *ACS Appl.*  
3 *Mater. Interfaces* **2016**, *8*, 32401-32407.
- 4 [24] Graedel, T. E.; Franey, J. P.; Gualtieri, G. J.; Kammlott, G. W.; Malm, D. L. On the  
5 Mechanism of Silver and Copper Sulfidation by Atmospheric H<sub>2</sub>S and OCS. *Corros. Sci.* **1985**,  
6 *25*, 1163-1180.
- 7 [25] Galtayries, A.; Bonnelle, J.-P. XPS and ISS Studies on the Interaction of H<sub>2</sub>S with  
8 Polycrystalline Cu, Cu<sub>2</sub>O and CuO Surfaces. *Surf. Interface Anal.* **1995**, *23*, 171-179.
- 9 [26] Reid, M.; Punch, J.; Ryan, C.; Garfias, L. F.; Belochapkine, S.; Franey, J. P.; Derkits, G. E.;  
10 Reents, W. D. Microstructural Development of Copper Sulfide on Copper Exposed to Humid H<sub>2</sub>S.  
11 *J. Electrochem. Soc.* **2007**, *154*, C209-C214.
- 12 [27] Sansregret, J. L. Reaction of Copper Oxide with H<sub>2</sub>S. *J. Electrochem. Soc.* **1980**, *1*, 2083.
- 13 [28] Adhikari, S.; Sarkar, D.; Madras, G. Hierarchical Design of CuS Architectures for Visible  
14 Light Photocatalysis of 4-Chlorophenol. *ACS Omega* **2017**, *2*, 4009-4021.
- 15 [29] Minceva-Sukarova, B.; Najdoski, M.; Grozdanov, I.; Chunnillall, C. J. Raman Spectra of Thin  
16 Solid Films of Some Metal Sulfides *J. Mol. Struct.* **1997**, *410-411*, 267-270.
- 17 [30] Kumar, P.; Nagarajan, R. An Elegant Room Temperature Procedure for the Precise Control  
18 of Composition in the Cu–S System. *Inorg. Chem.* **2011**, *50*, 9204-9206.

- 1 [31] Mondal, G.; Bera, P.; Santra, A.; Jana, S.; Mandal, T. N.; Mondal, A.; Seok, S. I.; Bera, P.  
2 *New J. Chem.* Precursor-Driven Selective Synthesis of Hexagonal Chalcocite (Cu<sub>2</sub>S) Nanocrystals:  
3 Structural, Optical, Electrical and Photocatalytic Properties. **2014**, 38, 4774-4782.
- 4 [32] Huang, K.-J.; Zhang, J.-Z.; Fan, Y. One-Step Solvothermal Synthesis of Different  
5 Morphologies CuS Nanosheets Compared as Supercapacitor Electrode Materials. *J. Alloy. Compd.*  
6 **2015**, 625, 158-163.
- 7 [33] Karikalan, N.; Karthik, R.; Chen, S.-M.; Karupiah, C.; Elangovan, A. Sonochemical  
8 Synthesis of Sulfur Doped Reduced Graphene Oxide Supported CuS Nanoparticles for the Non-  
9 Enzymatic Glucose Sensor Applications. *Sci. Rep.* **2017**, 7, 2494 (1-10).
- 10 [34] Estrada, A.; Silva, F.; Soares, S.; Coutinho, J.; Trindade, T. An Ionic Liquid Route to Prepare  
11 Copper Sulphide Nanocrystals Aiming at Photocatalytic Applications. *RSC Adv.* **2016**, 6, 34521-  
12 34528.
- 13 [35] Du, Y.; Yin, Z.; Zhu, J.; Huang, X.; Wu, X.-J.; Zheng, Z.; Yan, Q; Zhang, H. A General  
14 Method for the Large-scale Synthesis of Uniform Ultrathin Metal Sulphide Nanocrystals. *Nat.*  
15 *Commun.* **2012**, 3, 1177 (1-7).
- 16 [36] Cruz, J.; Hernandez, S. A.; Delgado, F.; Angel, O.; Perez, R.; Delgado, G. Optical and  
17 Electrical Properties of Thin Films of CuS Nanodisks Ensembles Annealed in a Vacuum and Their  
18 Photocatalytic Activity. *Int. J. Photoenergy* **2013**, 2013, 178017 (1-9).
- 19 [37] Jia, L.; Lai, J.; Wang, J.; Chen, H.; Zheng, X.; Liu, H.; Jin, Z. Morphology, Structure and  
20 Optical Absorption Properties of Copper Sulfides by Different TEG Based Solution Processing.  
21 *Mater. Des.* **2017**, 123, 39-45.

- 1 [38] Li, S.; Zha, T.; Wang, Q; Wang, C.; Ren, Y.; Chen, Y.; Pan, D. Facile Fabrication of p-Type  
2  $\text{Cu}_x\text{S}$  Transparent Conducting Thin Films by Metal Sulfide Precursor Solution Approach and Their  
3 Application in Quantum Dot Thin Films. *J. Alloys Compd.* **2017**, *716*, 278-283.
- 4 [39] Dexter, M.; Gao, Z.; Bansal, S.; Chang, C.-H.; Malhotra, R. Temperature, Crystalline Phase  
5 and Influence of Substrate Properties in Intense Pulsed Light Sintering of Copper Sulfide  
6 Nanoparticle Thin Films. *Sci. Rep.* **2018**, *8*, 2201.
- 7 [40] Ellmer, K. Past Achievements and Future Challenges in the Development of Optically  
8 Transparent Electrodes. *Nat. Photonics* **2012**, *6*, 809-817.
- 9

# 1 Table of Contents



2